J. Fluid Mech. (1989), *vol.* 204, *pp.* 523–542
Printed in Great Britain

Secondary flows and vortex formation around a circular cylinder in constant-shear flow

By H. G. C. WOO, J. E. CERMAK AND J. A. PETERKA
Department of Civil Engineering, Colorado State University, Fort Collins, CO 80523, USA

(Received 3 March 1988 and in revised form 8 February 1989)

A pair of curved gauzes with non-uniform porosity was used to generate a strong constant-shear flow with low turbulence intensity. The complex features of this flow around a circular cylinder with its axis normal to the vorticity and mean velocity vectors were studied. Methods such as the use of end plates, inclusion of gaps at the junctions of the cylinder with the end plates, and fluid withdrawal were applied to minimize end effects. Exploratory studies were made to investigate shear effects on the vortex-wake formation region with Reynolds numbers between 800 and 1.4×10^4. Effects of the steepness factor on vortex formation were explained by regarding secondary flow in the base region of the cylinder as negative base bleeding which behaves as a wake interference element.

1. Introduction

The flow field around a circular cylinder placed vertically in a shear flow with horizontal vorticity and mean velocity as illustrated in figure 1 is complex. Some theoretical and experimental examinations of the more general type of problem of flow about a strut when the approaching velocity varies in the spanwise direction have been reported by von Kármán & Tsien (1945), Squire & Winter (1951), and Hawthorne (1954). The analysis of this type of flow is generally based on an inviscid approximation, which regards the three-dimensional flow as a perturbation of the initial quasi-two-dimensional approaching flow and neglects wake effects. Experimental results of the foregoing authors have indicated that distortion of the flow due to presence of the body tends to be considerable. Hawthorne has shown that the nose-profile shape of the strut influences the size of the three-dimensional disturbances appreciably. A round nose strut causes such a large disturbance that the small perturbation assumption used in the theoretical analysis is invalidated.

In laboratory studies of a circular cylinder in constant-shear flow, both the cylinder and the shear flow are confined between the walls of the tunnel and are necessarily of finite extent. In the first part of this paper, the spanwise secondary flows and end-effect problems caused by these three-dimensional disturbances due to confinement of the cylinder and the shear flow are presented and discussed.

For a bluff body in a stream, the importance of the wake region when organized vortices are formed, as well as the close relationship between the flow dynamics in this region and the fluid-induced force on the bluff body, have been recognized for quite some time. Roshko (1954) has discussed the importance of the vortex dynamics on the cylinder base pressure and the cylinder drag. Bloor (1963), Gerrard (1965, 1966), and others have studied intensively the cylinder wake from a basic perspective. Among the numerous publications on this subject, one thing in common is that they are all restricted to bodies in uniform flow. There is no quantitative work existing at

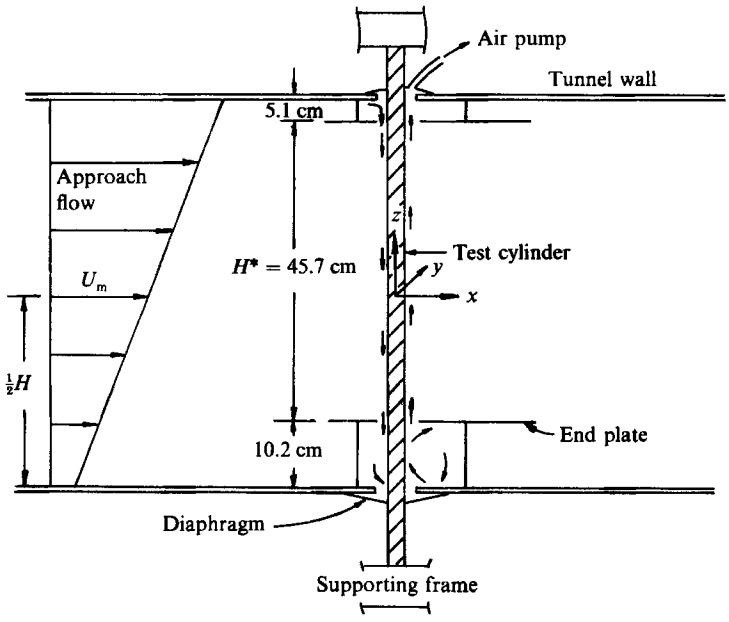

FIGURE 1. Diagram of test arrangement.

present that is related to shear effects on the vortex-wake formation. In the second part of this paper, results of exploratory measurements of some of the characteristcs associated with a vortex wake for a circular cylinder in constant-shear flow are reported. The results presented in the second part are a quantitative supplementation to results presented in the first part where the highly three-dimensional characteristics of secondary flows around the test cylinder have been discussed qualitatively.

2. Design of experiments

2.1. *Constant-shear flow in a wind tunnel*

The constant-shear flow was generated by means of a pair of curved gauzes with non-uniform porosity. The basic concept and considerations that led to the development of such a device have been described in detail by Woo *et al.* (1989). The wind tunnel used for this study is of open-return type which has a cross-section of 61 cm × 61 cm and a test section length of 244 cm. The shear-flow generator was installed at the upstream section of the tunnel immediately following a fine honeycomb block of 5 cm in thickness at the inlet to create a uniform, low-turbulence approach flow. The velocity distribution outside the wall boundary layers at the test section, as shown in figure 2, varies almost linearly from $1.8U_m$ at the ceiling of the tunnel to about $0.3U_m$ at the floor, where U_m is the mean velocity at midheight of the tunnel. The shear flow thus has a shear parameter λ of 1.5 where λ is defined as follows: $U/U_m = 1 + \lambda z/H$. In this definition z is the vertical coordinate centred at midheight of the tunnel, and H is the height of the tunnel.

The wind tunnel is driven by a 15 HP constant-speed motor. Vibration caused by the wind-tunnel fan is effectively eliminated by a flexible vibration-damping connection between the fan and the test section. Variation of the flow speed was

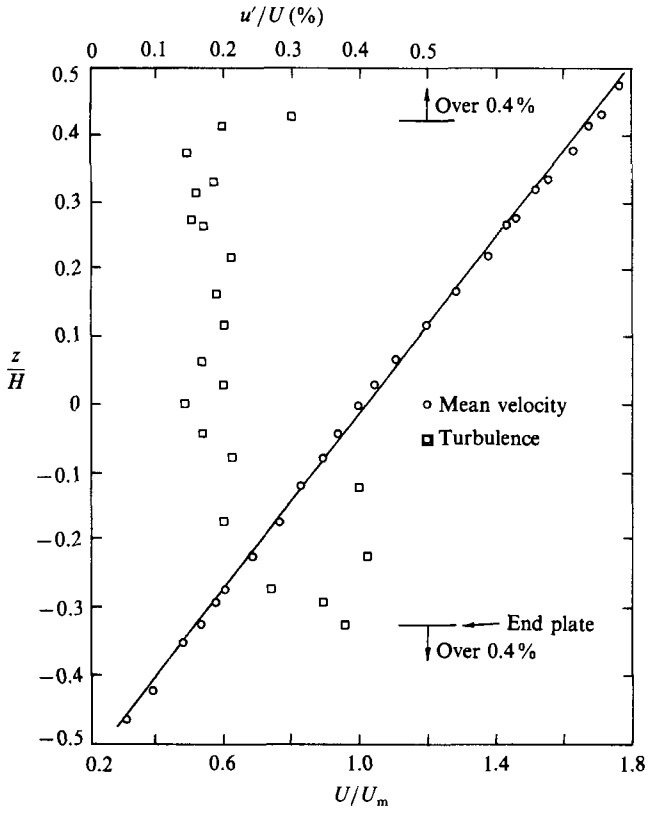

FIGURE 2. Mean velocity and turbulence-intensity distribution at the test section.

obtained by remotely adjusting the pitch of the fan blades. It was found that the shear-flow velocity distribution did not change significantly either over the span of the test section or with the wind speed over the range used for the studies ($1.4\ \text{m/s} \leqslant U_m \leqslant 6.7\ \text{m/s}$). As the wind tunnel is of the open-return type, small fluctuations of air pressure in the laboratory influenced the flow in the working section when the tunnel was operated at low speed. It was found that with a wind speed at the test section of not less than 1.4 m/s and with a relatively calm laboratory environment, a well-developed constant-shear flow with steady test conditions could be maintained. The flow encounters considerable pressure loss when it passes through the pair of curved gauzes. With the available drive motor, the maximum speed that could be achieved at midheight of the tunnel was 6.7 m/s. The local turbulence level in the region $-0.33 \leqslant z/H \leqslant 0.42$ was between 0.2 and 0.4%. Flow visualization indicated that the streamlines were parallel at the test section. Results of the static pressure measurements showed that it was essentially constant throughout the test section.

2.2. *Experimental methods and procedures*

Measurements of both the mean and fluctuating velocites were made with a quartz coated constant-temperature hot-film probe. Mean and root-mean-square values of the anemometer bridge output were obtained by one-minute averaging. The method suggested by Bearman (1970) was used to correct the error due to temperature

differences between calibration and measurement. The traverse mechanism supporting the hot-film probe permitted accurate positioning of the probe to within 0.5 mm.

Vortex-shedding frequency measurements were made with a sound and vibration analyser. The analyser has a range from 2.5 c.p.s. to 25 k.c.p.s. in four decade ranges. The analyser filter was set at $\frac{1}{10}$ octave which had at least 40 db attenuation at one-half and twice the selected frequency. Thus, the analyser output could be used to accurately detect frequencies containing high energy. The analyser outputs were recorded on chart paper. Measurements of the vortex-shedding frequency were obtained by placing the hot-film probe at a position just outside the turbulent wake such that it would sense the velocity fluctuations due to the vortex shedding. This position was generally at a distance of about $1.0D$ downstream of the base of the test cylinder and about $2.0D$ laterally (y-direction) from the wake centreline, where D is the cylinder diameter.

Cylinder surface-pressure measurements were performed with 0.12 cm diameter pressure taps which were connected to a Baratron pressure-measuring head.

Flow-visualization studies were performed by bleeding smoke through small holes on the surface of the test cylinder. Special care was taken so that the relative velocity between the smoke from these small holes and local flow over the cylinder was minimized. The smoke was generated using a simple apparatus which forced the burning of low-tar tobacco with compressed air. The smoke was filtered and cooled before it reached the test cylinder. The flow pattern was captured either with Polaroid film or with a high-speed movie camera.

Brass tubes of five different diameters (0.64, 1.27, 1.91, 2.54, and 3.81 cm) were used as the test cylinders. The surfaces of the tubes were all carefully polished with fine steel wool. A quantitative evaluation of the surface roughness was not considered necessary. The cylinder was directly supported by a heavy steel frame which was set on the floor and had no direct contact with the wind tunnel. Rubber diaphragms were used to prevent air leaking at the junctions of the cylinder with the tunnel (figure 1).

For the test cylinders, the wind-tunnel blockage ratio ranged from 1.0 to 6.3%. In order to have a better comparison of the data, it was desirable to make some attempt to correct the results for blockage. The theory proposed by Maskell (1965) was used to correct the stream velocity. The values of $\Delta U/U$ are given by $0.006D/0.64$, where D is measured in cm.

The initial position of the fully formed vortex defines the end of the formation region. A list of the criteria that are used to locate the end of the vortex-formation region can be found in Griffin & Votaw (1972). According to Griffin & Votaw some of the criteria yield essentially the same value for the vortex-formation length L_f. The criterion proposed by Bloor & Gerrard (1966) was adopted in this study. Thus, the position of the maximum turbulence level ($u'/U_m \times 100$) at twice the vortex-shedding frequency on the wake axis was defined as the end of the vortex-formation region. The length of the vortex-formation region was determined by hot-film probe traversing along the wake axis. The output of the hot-film anemometer was connected to a band-pass filter with centre frequency set at $2f_s$. The fluctuating velocity was subsequently read on an r.m.s. meter. Once the location of the end of the vortex-formation region was found, the wake width D' at that particular location was obtained by searching for the point of maximum wide-band longitudinal turbulence intensity across the wake in the y-direction. The positions of this maximum velocity fluctuation, as has been discussed by Bearman (1965), are coincident or near coincident with positions of vortex centres. 'To a first approximation at least,'

Bearman argues, 'it can be said that downstream of vortex formation, positions of maximum velocity fluctuations taken from traverses across the wake, give the lateral spacing of the vortices.' Consequently, this lateral spacing between the maxima of velocity fluctuations at the end of the vortex-formation region has been defined as wake width by authors such as Griffin & Votaw, and Griffin & Ramberg (1974).

3. Results and discussion

3.1. *Secondary flows, end effects and base pressure*

3.1.1. *Secondary flows*

The origin of secondary flows around a circular cylinder spanned across a constant shear flow has been demonstrated by Starr (1966). Take a_1–b_1 as the tyical streamline around the cylinder (figure 3). As the flow approaches the cylinder, the streamline is first deflected in a direction away from the cylinder in the region a_1. As the flow proceeds the streamline is deflected back to approximately its former direction in the region b_1. Considering the flow outside the boundary layer and wake region around the cylinder as inviscid and incompressible, based on a quasi-two-dimensional analysis, Starr showed the existence of a pressure gradient in the positive z- direction in the region a_1 upstream of the streamline inflection point. In the region b_1, a similar mechanism produces a pressure gradient in the negative z- direction. The greater the curvature of the streamline the stronger is the pressure gradient.

For flow within the boundary layer or the separated wake region, the secondary flow can still be regarded as due to variations in pressure. Along the front stagnation line of the cylinder, the stagnation pressure is higher at the high-velocity end of the cylinder than that at the low-velocity end. On the lee side of the cylinder in the wake region, the entrainment rate of the separated free shear layer is higher at the high-velocity end than that at the low-velocity end. This is because in the subcritical range, as the location of transition from laminar to turbulent flow moves from the end of the vortex-formation region toward the cylinder, the relative length of turbulence in the separated free shear layer increases. According to Gerrard (1966), the rate of entrainment between the separated shear layers is governed mainly by the length of the turbulent shear layers. Variation of the entrainment rate should result in changes of the vortex strength as well as size of the vortex-formation region and the cylinder base pressure. At the high-velocity end, the length of the turbulent shear layer should be greater than that at the low-velocity end. Therefore, the entrainment rate should be higher at the high-velocity end. Consequently, base pressure at the high-velocity end is lower than that at the low-velocity end. Spanwise secondary flows around the cylinder are induced due to the existence of these pressure gradients (figure 1). These spanwise secondary flows convert the relatively simple incident flow into a complex three-dimensional flow with velocities normal to the main flow which persist downstream of the cylinder.

A case study was conducted to study visually these spanwise secondary flows. The cylinder used had a diameter of 1.27 cm and a steepness factor relative to the incident shear flow β_m of 0.034, where β_m is defined as $\beta_m = (\mathrm{d}U/\mathrm{d}z)\,(D/U_m) = \lambda\, D/H$. The Reynolds number based on midheight tunnel speed U_m was 960. Two frames of the ciné film (the camera was operated at 560 frames/s) with a time difference of 0.1 s which show the secondary flow on the lee side of the cylinder in the base region are shown in figure 4. The elevation z/D at which the smoke was released is -2. Following a specific packet of smoke, as shown in the pictures (indicated by

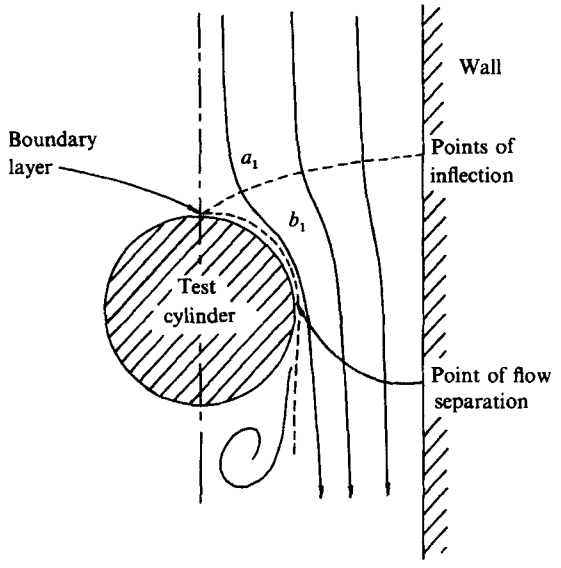

FIGURE 3. Motion of fluid relative to a circular cylinder.

arrows), it can clearly be seen that the smoke is carried upward along the rear face of the cylinder by the spanwise secondary flow. The secondary flow was found to have a fluctuating velocity. This phenomenon is apparently caused by fluctuations of pressure due to periodic vortex shedding. By tracing about ten individual eddies from different segments of the film, the upward mean flow speed was calculated based on the distance a particular eddy travelled in a particular time interval. It was found for this case that the speed was as high as $0.44U_{\mathrm{m}}$.

Based on the work of Toomre (1960) for an infinite cylinder in a weak constant-shear flow, the magnitude of cross-flow along the leading edge of the cylinder should reach a maximum of around $0.04U_{\mathrm{m}}$ at a distance of about $0.025D$ in front of the cylinder. This velocity componenet rapidly vanishes at the surface of the cylinder because of the non-slip condition. The small magnitude of the cross-flow and the short distance away from the cylinder make it impossible for a fluid particle to travel much distance downward ($\Delta z/D$) before passing around the cylinder. Thus an attempt to obtain flow information by introduction of a smoke tracer was unsuccessful.

3.1.2. *End effects*

Based on a simple consideration of mass conservation, it is clear that the upward velocity component on the lee side of the cylinder will induce a recirculation bubble at the lower end of the cylinder (i.e. with a flow induced in the $-x$-direction near the lower boundary downstream of the cylinder), if the junction between the cylinder and the wind-tunnel wall (or end plate) is completely tight. This recirculation bubble can be seen in figure 5(*a*). In figure 5, smoke is emitted from a series of small holes on one side of the cylinder. The vortices shed from the cylinder appear to form continuous filaments and peel off from the high-velocity end. The recirculation bubble is at the bottom. As the flow proceeds upward toward the upper 'dead end', it will gradually be slowed down owing to an adverse pressure gradient. This effect is augmented by the downwash velocity component induced by a horseshoe vortex,

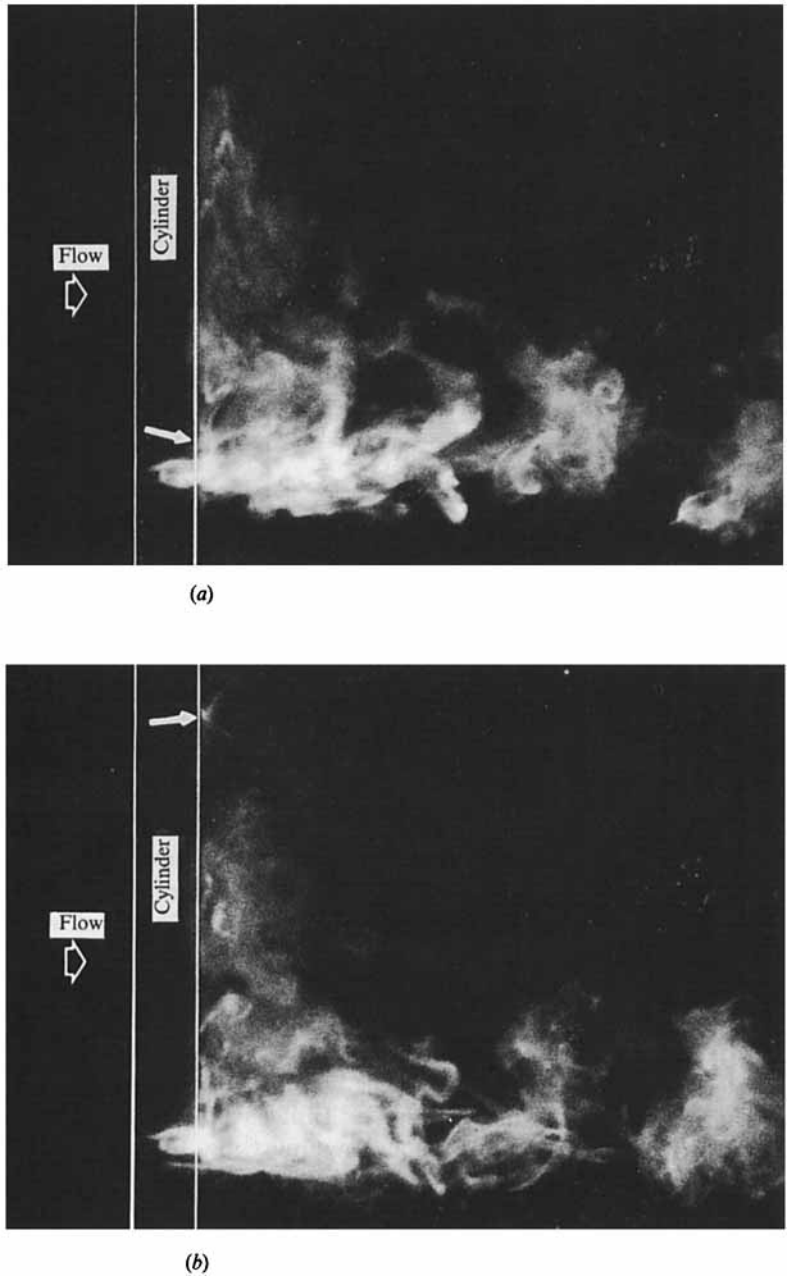

FIGURE 4. Secondary flow on the lee side of a cylinder with $D = 1.27$ cm, $\beta_m = 0.034$ and $Re_m = 960$ (the arrows point to a traced packet of smoke): (*a*) at time $t = 0.0$ s (*b*) $t = 0.1$ s.

which will be discussed later. At the point where the upward flow velocity is sufficiently retarded, the flow will separate from the surface of the cylinder. Consequently, a recirculation bubble will also exist at the upper end of the cylinder on the lee side. This upper-end, lee-side recirculation bubble is shown in figure 5(*b*). At the leading edge of the cylinder the recirculation bubble should also exist at both ends. However, owing to the periodic shifting of the front stagnation line caused by

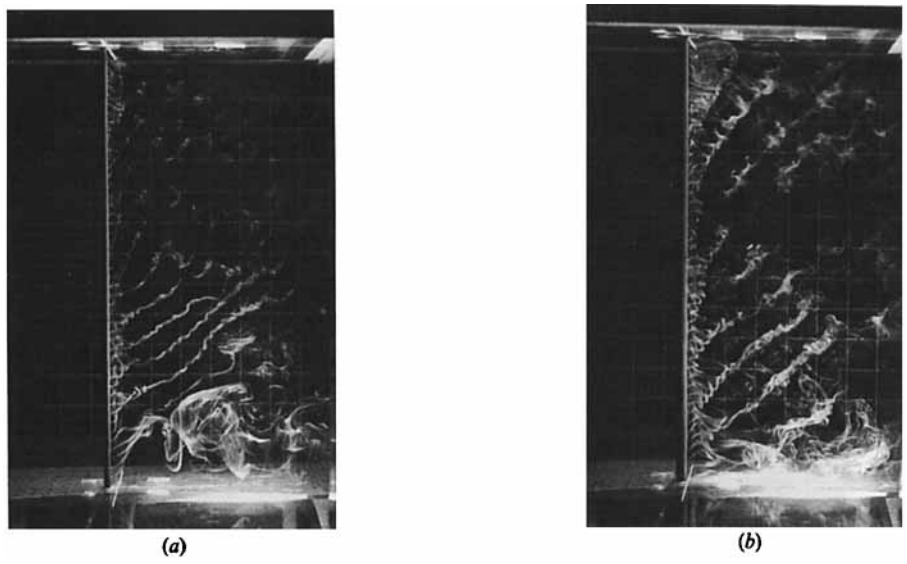

FIGURE 5. End effect at junctions of the test cylinder and tunnel walls: (*a*) the lower separation bubble, (*b*) the upper separation bubble.

vortex shedding (Toebes 1969) and the curved surface of the cylinder, the scales of the recirculation bubbles are so small and unsteady that they are practically unobserveable. Since a shear flow generated in the laboratory is necessarily of limited extent, laboratory studies of flow around a cylinder in shear flow will always have this type of end-effect problem.

The effect of boundary layers on the wind-tunnel walls on cylinder base-pressure measurement has been discussed by Stansby (1974), who showed that a reduction of boundary-layer thickness caused a reduction of base pressure. As has been discussed by Mair & Stansby (1975), this effect is believed due to a flow of slow-moving fluid from the wall boundary layer into the base region of the cylinder. Stansby pointed out that most of the published pressure distributions for circular cylinders were obtained without end plates and this probably explained their inconsistency. A common practice for eliminating the end effect caused by wind-tunnel boundary layers is to use an end plate which makes the boundary layer at the inner face of the end plate and junction with the cylinder as thin as possible. In this way, a test condition that is very nearly two-dimensional may be achieved in the uniform-approach-flow case. However, if the approach flow is sheared and no space exists between the end plates and cylinder, the recirculation-bubble end effect just mentioned will result. The stronger the shear flow, the worse is the problem.

In the constant-shear-flow case, in addition to the end effects caused by the spanwise secondary flows and boundary layers, there is a third kind of end effect caused by the horseshoe vortex. In an undisturbed constant-shear flow, vortex lines are all normal to the plane of the flow. As the shear flow approaches the cylinder, the vorticity vector is progressively turned until eventually vortex lines near the body are bent into the flow direction. At both ends of the cylinder, the vorticity accumulates and forms into what are generally known as horseshoe vortices. These two horseshoe vortices are formed from a different source than the two horseshoe vortices caused by the boundary layers on the ceiling and floor of the tunnel. At the

floor of the tunnel, the horseshoe vortex due to the constant-shear flow has the same sign as that caused by the lower boundary layer. Most likely, they merge and become indistinguishable. However, at the ceiling of the tunnel, the horseshoe vortex from the boundary layer and the horseshoe vortex from the constant-shear flow are of opposite sign. Their relative sizes should be related to thickness of the boundary layer and the strength of the constant-shear flow. The streamwise vorticity at each side of the cylinder will induce a downward velocity component in the base region of the test cylinder. In the present case, this downward velocity component can be quite high at both ends of the cylinder, owing to the strength of the constant-shear flow and the considerable vorticity accumulation.

With the present experimental set-up, the boundary-layer thickness at the tunnel ceiling is about 1.3 cm and at the floor is about 3.8 cm. The upper end plate was installed at 5.1 cm from the ceiling and the lower end plate was installed at 10.2 cm from the floor. This arrangement is based on the practical consideration that the local turbulence intensity within the effective test height would be less than 0.4%. The distance H^* between the inner faces of the end plates is considered as the effective wind-tunnel height. The dimensions of the rectangular end plate are 26.7 cm in width, 28.6 cm in length, and 0.32 cm in thickness. Design of the end plates was based on the results from the optimization experiments by Stansby (1974). Stansby proposed a width of $7.0D$, about $2.0D$ from the leading edge of the end plate to the cylinder, and $4.5D$ from the trailing edge of the end plate to the cylinder. For this study D was taken as 3.81 cm, the largest cylinder used in the study. The leading edges of the end plates were sharpened to minimize the disturbances.

Owing to the high strength of the shear flow generated, the spanwise secondary flows and the horseshoe vortices are all quite strong. After some consideration, it was decided to leave some gaps between the cylinder and the end plates. In addition to this, at the top end of the cylinder on the lee side, an air pump was used to reduce the local pressure at the 'dead end' by continuous removal of air. Therefore, a smooth and continuous passage for the spanwise secondary flows at both the upstream side and the downstream side of the cylinder could properly be maintained. These arrangements are shown in figure 1. It is believed that with these arrangements, there should be no effect of the boundary layers on the inner faces of the end plates. However, two horseshoe vortices of the same sign should still exist there. For each test cylinder at different tunnel speed, the gaps and the extraction rate of the air pump were adjusted separately by introducing smoke into the flow field and observing the wake pattern. Flow visualization showed that with these arrangements, it was possible to effectively eliminate the recirculation bubbles between the end plates. The effect caused by the upper boundary layer which existed on the ceiling of the tunnel was consequently completely eliminated by the air pump. The same method could have been used at the lower end of the cylinder to prevent higher pressure flow from the boundary layer on the floor of the tunnel from flowing upward into the base region of the test cylinder. It was based on the consideration that the lower horseshoe vortices, which existed on both faces of the lower end plate, all induced a downwash velocity component in the base region of the cylinder, namely, the lower horseshoe vortices having exactly the opposite effect on the base region of the cylinder as the lower boundary layer. Without using an air pump these two effects were left to counterbalance each other across the cylinder end-plate gap.

The merit of these arrangements to reduce the end effects shall be seen in the results of base-pressure measurements which will be discussed in the following section.

3.1.3. *Base pressure*

For a circular cylinder spanned across a constant-shear flow generated in the laboratory, if the flow is incompressible, then the base pressure coefficient based on local velocity should be a function of the kinematic viscosity ν, the local incident velocity U, the cylinder diameter D, the velocity gradient of the incident flow $\mathrm{d}U/\mathrm{d}z$, and the spanwise position z. The involvement of spanwise position z should be interpreted as the result of base-pressure variation caused by the end effects. Based on a simple dimensional analysis, the local base-pressure coefficient C_{pb_ℓ} can be formulated as

$$C_{pb_\ell} = F(\mathrm{Re}_\ell, \beta_\ell, z/D), \tag{1}$$

where $Re_\ell = UD/\nu$, and $\beta_\ell = (\mathrm{d}U/\mathrm{d}z)\,(D/U)$.

For a shear flow with moderate strength or of relatively limited extent, spanwise variations of local Reynolds number and local steepness factor are small and can be neglected. Furthermore, if the H^*/D ratio is large enough, then the test conditions near the central section of the cylinder may be expected to be free from end effects. Therefore, according to Mair & Stansby (1975) Re_ℓ and β_ℓ may be replaced by a mean value, i.e. the value at midspan, to give

$$Re_\mathrm{m} = \frac{U_\mathrm{m} D}{\nu}, \quad \beta_\mathrm{m} = \frac{\mathrm{d}U}{\mathrm{d}z}\frac{D}{U_\mathrm{m}}.$$

Therefore, the base-pressure coefficient may be expressed as follows:

$$c_{pb_\ell} = f(Re_\mathrm{m}, \beta_\mathrm{m}). \tag{2}$$

Measurements of base pressure were made at various spanwise position on circular cylinders of diameter 1.27 cm, 1.91 cm, and 2.54 cm. The local base-pressure coefficient C_{pb_ℓ} is defined as $(P_\mathrm{b}-P_\infty/(0.5\ \rho U^2)$ where P_b is the local mean base pressure, P_∞ is the static pressure of the undisturbed flow, and U is the local corrected free-stream velocity. The pressure measurements reported in this section were taken with the tunnel running only at speed $U_\mathrm{m} = 2.80$ m/s. Results of these base-pressure measurements are shown in figure 6. The related parameters for these measurements are shown in table 1. The base-pressure distributions along each test cylinder follow the same pattern – at the top of the cylinder there is a high-pressure region, at the lower end of the cylinder there is a low-pressure region, and in between these two regions the pressure coefficient is essentially constant.

As has already been mentioned, the streamwise vorticity at each side of the cylinder will induce a downward velocity component in the base region all along the cylinder. This vertical velocity component can be quite high at both ends of the cylinder where concentrated vortices exist. At the lower end of the cylinder in the base region, both the flow induced by the pressure gradient, which is moving upward, and the flow induced by the concentrated vortex, which is moving downward, all act to direct the fluid away from the base region and therefore create a low-pressure region. At the upper end of the cylinder in the base region both flows serve to bring fluid into that region. Two streams converge and therefore create a higher pressure region. In between these two regions the local flow conditions are relatively free from the effects coming from both ends. The base-pressure coefficient is essentially constant for each test cylinder in the central region. That is, the local base-pressure

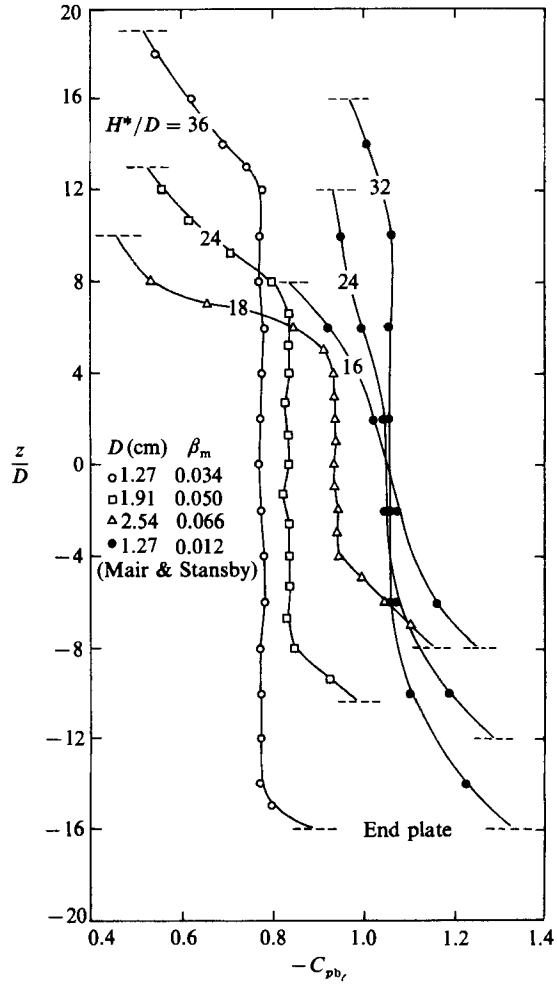

FIGURE 6. Distribution of base-pressure coefficient of a circular cylinder in constant-shear flow.

D(cm)	H^*/D	β_m	Re_m	Re_ℓ†	β_ℓ†	$-C_{pb_\ell}$
1.27	36	0.034	1980	1180–3040	0.023–0.058	0.78
1.91	24	0.050	3000	2060–4250	0.038–0.076	0.84
2.54	18	0.066	4020	3000–5330	0.052–0.094	0.94

† In the range where base-pressure coefficient is essentially constant.

TABLE 1. Results of base-pressure measurements along the cylinder axis and the related parameters

coefficient is not affected by the variation of Re_ℓ and β_ℓ and is independent of z/D. Namely, there is a region at the central section of each test cylinder where (2) applies. However, there is a systematic shift in the values for different test cylinders. This phenomenon cannot be caused by variations of the H^*/D ratio. As has been shown by Mair & Stansby (1975) (some of their results are included in figure 6), variation of H^*/D will affect only the extent of the central region that is free from the domination of end effects, while it does not cause any detectable shifting of the base-

pressure coefficient at the central region. Closer examination indicated that variations of extraction rate of the air pump did not result in shifting of the base-pressure coefficient either. Therefore, this shifting in base-pressure coefficient is apparently due to the differences in Re_m and β_m values for each test cylinder. Effects of Reynolds number and steepness factor on the local base-pressure coefficient will be discussed in more detail in the next section in conjunction with the wake-characteristic measurements.

The H^*/D ratios for the test cylinders as shown in table 1 and figure 6 are 36, 24, and 18, respectively. The corresponding relative extent of constant base-pressure coefficient is $26D$, $15D$, and $8D$. This corresponds to real lengths of 33 cm, 28.6 cm, and 20.3 cm. The process of coalescence of incident vorticity into a concentrated vortex depends not only on the shape of cylinder but also on the time D/U for the vorticity to coalesce. In other words, as the cylinder diameter is increased, the relative size of the horseshoe vortices at both ends of the cylinder should also grow. This directly results in a smaller region at the middle section where the base-pressure coefficient is constant.

It is quite evident that the present experimental arrangements shown in figure 1 have not resulted in the complete elimination of end effects. However, if the present results of base-pressure measurement are compared with those of Mair & Stansby (1975), where no gap existed at the junctions of the cylinder and end plates, considerable improvement can be observed. In spite of the fact that the shear flow used in this study ($\lambda = 1.5$) is almost four times as strong as that used by Mair & Stansby ($\lambda = 0.4$), for the $H^*/D = 24$ case, the extent of the region where the base-pressure coefficient is constant is increased from $4D$ to $15D$. In the case of Mair & Stansby, the results indicate that when $H^*/D \leqslant 20$ the entire flow field in the base region of the cylinder is a 'ected by the separation bubbles. It is believed that the same situation also occurred in the experimental arrangement of Maull & Young (1973) in which a model with a semi-elliptic nose followed by a long parallel-sided section and blunt base was used. The separation bubbles should be more likely to occur for a model like this than for a circular cylinder.

Because a relatively strong constant-shear flow was used in this study, as illustrated in table 1, wide variations in both Re_ℓ and β_ℓ along the span of the test cylinders were obtained. The form of vortex shedding behind the test cylinders has also been found by the present authors (Woo *et al.* 1989) to break down into a number of cells for each of which the frequency is constant. Maull & Young (1973) have reported that the boundaries between the vortex cells coincide with points of inflection (or changes of slope) in the C_{pb_ℓ} curve. Mair & Stansby (1975) have also mentioned these irregularities in the C_{pb_ℓ} curves at the cell boundaries. These irregularities in the C_{pb_ℓ} curves appear to be less marked, in the case of cell boundaries less well defined, with the short D-section model and circular cylinder than with the long D-section model.

It is suggested by Maull & Young (1973) that a longitudinal trailing vortex, formed by amalgamation of the inital vorticity in the approaching stream as the vorticity is bent around the cylinder into the flow direction, makes the boundary of each vortex cell. In a later study, Woo *et al.* (1989) have concluded that these spanwise distributed vortices have a deterministic role in the cellular flow pattern behind a test cylinder. Mair & Stansby (1975) speculate that the length of the cylinder in the stream direction may be important in relation to the time needed for the vortex lines at different spanwise positions to coalesce. This speculation has also been confirmed in the experimental results of Woo *et al.* (1989) which show that under the same test

conditions, circular cylinders with larger diameters tend to generate more clearly defined vortex cells than circular cylinders with smaller diameters The same effect can also be seen in figure 3 of the paper by Maull & Young, which shows results of base-pressure measurements in (apart from the boundary layers) uniform flow. The vorticity in the boundary layers has coalesced into horseshoe vortices and their scales have become of such large extent that they dominate two thirds of the flow field in the base region.

In the present study, most likely the streamwise trailing vortices were not strong enough to cause any detectable wavy pattern in the base-pressure distribution by the pressure transducer used. Another possibility is that the flow field was sufficiently unstable that any pattern of variation in mean base pressure was obscured by pressure fluctuations. Owing to the small size of the wind tunnel and the strength of the spanwise secondary flow on the lee side of the test cylinders, the local base-pressure distribution as a whole is very much dominated by the secondary flow. Therefore, equation (2) for the base-pressure coefficient should be appropriate. Some changes in the base-pressure coefficient should be expected when H^*/D is very large and the spanwise variations of Re_ℓ and β_ℓ along the test cylinder are so large that they are no longer properly represented by values at the midheight of the tunnel.

3.2. *Wake-characteristic measurement*

The forward stagnation pressure, base pressure, vortex-shedding frequency as well as vortex-formation length and wake width at the end of the vortex-formation region were included in the measurements. The measurements were all conducted at midspan of the test cylinders only. An example, for the 2.54 cm diameter cylinder, of the results of hot-film measurements along the wake axis for the test cylinders at various speeds is shown in figure 7. The peak of the r.m.s. velocity curve marks the end of the vortex-formation region. The corresponding results of the wake-width measurements are shown in figure 8. Normalized results of the vortex-formation length L_{f} and wake width D' using the cylinder diameter D for the reference length are summarized and presented in table 2 together with the Strouhal number, the front and base-pressure coefficients and the related parameters of Reynolds number and the steepness factor.

For better comparison of shear effects, two cases of a circular cylinder in uniform flow were added to the test plan after completion of the shear-flow testing cycle. The results are included in table 2. In the uniform cases, the turbulence levels of the incident flow were the same as the shear-flow cases, which were 0.2%. Since the present Reynolds number range is between 800 and 1.4×10^4, the flow characteristics around the cylinder are very sensitive to both the Reynolds-number variations and the disturbance level of the free stream (Gerrard 1965, 1966). Therefore, it is important to have the same level of turbulence intensity.

For each test cylinder with an essentially constant steepness factor, the data in table 2 show that, except for the Strouhal number which practically remains the same, the vortex-formation length, the wake width and the base-pressure coefficient decrease as the Reynolds number increases. This tendency can more readily be seen in figure 9. The results of table 2 also indicate that an increase of the steepness factor has no significant effect on the wake-formation length, while it does cause an increase in the wake width and a decrease in both the base-pressure coefficient and the Strouhal number if the Reynolds number is kept approximately the same (figure 10). Based on some extrapolations of the test results, the cases in which the Reynolds number is approximately equal to 8000 are added to figure 10.

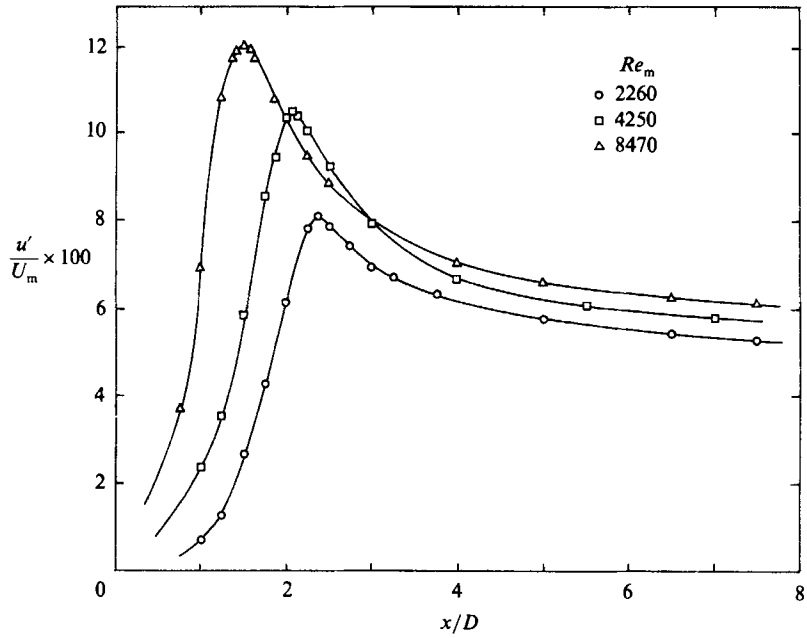

FIGURE 7. Turbulence level (r.m.s. fluctuations at twice the vortex shedding frequency/U_m) on the wake axis. $D = 2.54$ cm.

It has long been known that a significant reduction in the drag of an aerofoil with a blunt trailing edge can be achieved by interfering with the vortex-formation process in the wake with splitter plates or with ejection of fluid through the base of the aerofoil. Results on the changes that occur in the wake when a splitter plate or base bleeding is introduced can be found in the reports of Wood (1964), Bearman (1965, 1967) and Gerrard (1966). Comparisons of the present results with the results of the above-mentioned authors indicate some resemblance between effects of the spanwise secondary flow on the lee side of the cylinder and effects of the splitter plate or base bleeding upon the vortex-formation process.

It is quite obvious that the nature of the interference of the axial secondary flow on the vortex wake is quite different from that of base bleeding or splitter plates. The axial secondary flow is simply a convective motion due to the existence of a pressure gradient. Its scale and characteristics are determined mainly by the velocity variations along the cylinder axis and the state of the incident flow; i.e. a function of the steepness factor and Reynolds number. As for splitter plates and base bleeding, they are forced interferences on the vortex wake. Flow visualization reveals that the spanwise secondary flow is very much confined to the region well within the vortex-formation region in the immediate vicinity of the cylinder as shown in figure 4. The upward secondary flow on the lee side of the cylinder continuously extracts fluid from the base region. Thus, its effects should be equivalent to negative base bleeding and should result in a decrease of the base pressure. Therefore, it has exactly the opposite effect of positive base bleeding or a splitter plate.

Wood (1964) and Bearman (1965, 1967) have reported an increase of base pressure, vortex-formation length and the Strouhal number as the bleed rate or the length of the splitter plate is increased. With a sufficiently large bleed quantity or splitter-plate

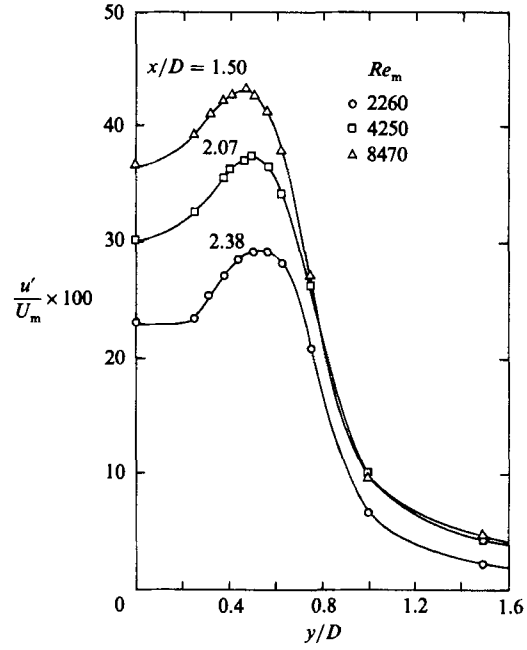

FIGURE 8. Turbulence intensity profile in the crosswise direction at the end of the vortex-formation region. $D = 2.54$ cm.

D(cm)	Re_m	β_m	L_f/D	D'/D	St	$-C_{pb_m}$	C_{pf_m}
0.64	1080	0.017	2.75	1.00	0.208	0.70	1.00
	2140	0.017	2.42	0.82	0.208	0.75	1.01
1.27	830	0.036	2.65	1.00	0.206	0.70	1.00
	1980†	0.034	—	—	—	0.78	—
	2260	0.034	2.33	0.86	0.200	0.80	1.00
	4380	0.034	2.05	0.82	0.201	0.90	1.01
	4730	0.034	1.92	0.82	0.202	0.92	1.01
	13000‡	0.012	—	—	—	1.05	—
1.91	2120	0.000‖	2.35	0.78	0.210	0.74	1.00
	2170	0.051	2.33	0.98	0.188	0.82	1.00
	3000†	0.050	—	—	—	0.84	—
	3170	0.050	2.15	0.92	0.193	0.85	1.00
	3880	0.050	2.05	0.88	0.190	0.90	1.00
	4300	0.050	2.02	0.87	0.191	0.92	1.00
	6900	0.050	1.62	0.84	0.191	1.02	1.01
2.54	2260	0.068	2.38	1.08	0.186	0.86	1.00
	4020†	0.066	—	—	—	0.94	—
	4190	0.000‖	2.00	0.74	0.208	0.88	1.00
	4250	0.066	2.07	1.00	0.184	0.97	1.00
	8470	0.066	1.50	0.94	0.187	1.16	1.04
3.81	4280	0.096	2.03	1.14	0.183	1.05	1.03
	7900	0.096	1.50	1.04	0.183	1.28	1.05
	14160	0.096	1.22	1.00	0.185	1.43	1.06

† From the results of figure 6.
‡ From the results of Mair & Stansby (1975).
‖ Uniform-flow result.

TABLE 2. Results of wake-characteristic measurements and the related parameters

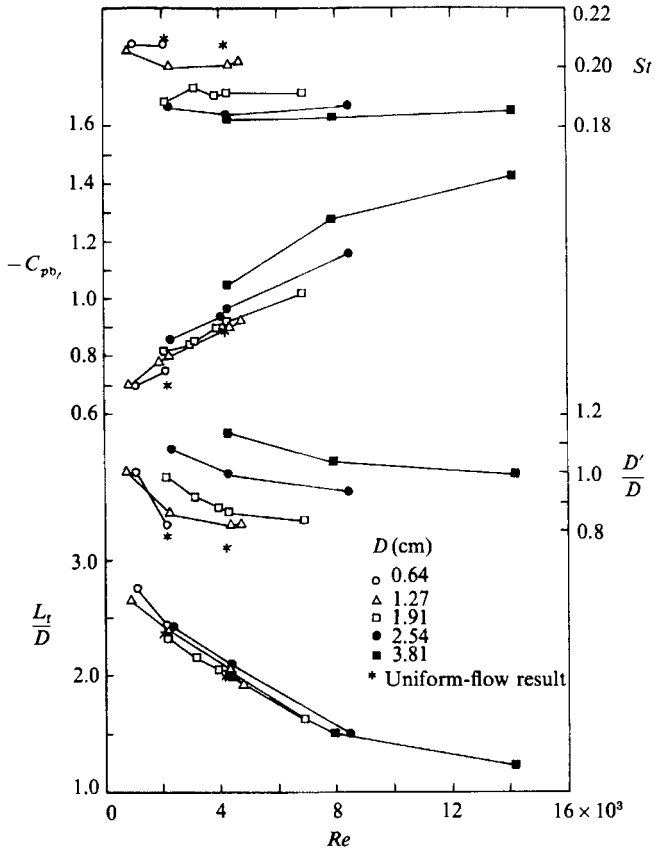

FIGURE 9. Variations of vortex-formation length, wake width, base-pressure coefficient, and Strouhal number with Reynolds number.

length, the vortex-formation process can be suppressed. However, they did not include the responses of the vortex-wake width to the interferences in their studies.

Present results indicate that for approximately constant Reynolds number, increasing the steepness factor has virtually no effect on the vortex-formation length. However, it does result in widening of the vortex wake and decreasing of the base-pressure coefficient. Thus, it is apparent that increasing the steepness factor will not only result in a widening of the scale of the secondary flow but also in an increase of the secondary flow speed. It is quite obvious that by holding β_m constant, increasing of Re_m will also increase the secondary flow velocity. Gerrard (1966) has pointed out that the size of the vortex-formation region is determined by the balance between entrainment into the shear layer and the replenishing of fluid by the induced reverse flow into the base region of the cylinder. Increasing the entrainment rate should result in, as indicated by the present results, not only a decrease of the wake width but also a substantial reduction of the vortex-formation length. Two separated free-shear layers are drawn closer together, which results in a lowering of the base pressure. Consequently, the spanwise pressure gradient and the pressure-gradient-induced secondary flow velocity should increase.

Since the secondary flow forces widening of the vortex wake and decreasing of the base pressure as indicated in figure 10, the base-pressure coefficient should be related to the vortex-wake width. Figure 11 is a graph of $-C_{pb'}$ against D/D' which shows

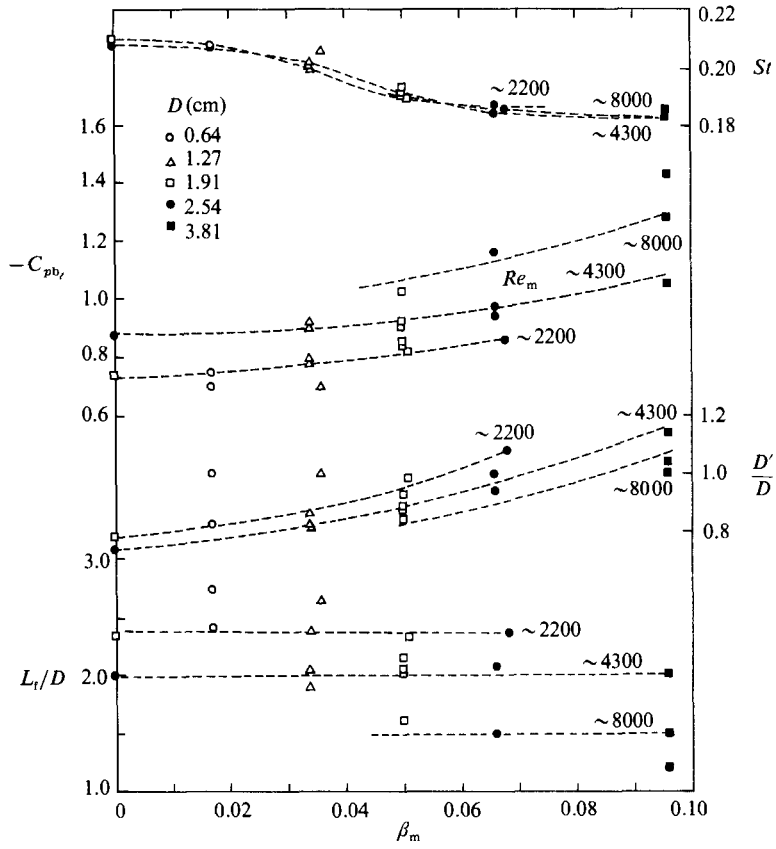

FIGURE 10. Variations of vortex-formation length, wake width, base-pressure coefficient, and Strouhal number with steepness factor.

a general dependency between these two parameters. The strong influence of Reynolds number is quite evident. If the base-pressure coefficient is plotted against the inverse of the vortex-formation length, as shown in figure 12, the results indicate that $-C_{pb_f}$ varies linearly with D/L_f. This result is in close agreement with the findings of Bearman (1965, 1967) that the length of the formation region is closely correlated with the pressure at the base of the cylinder. Figure 12 shows that if L_f goes to infinity $-C_{pb_f}$ would approach zero. If L_f approaches zero then $-C_{pb_f}$ would go to infinity – a situation not likely to occur in the shear-flow case owing to interference by the secondary flow. This situation could only be approached by controlled base suction which should completely destroy the vortex-wake-formation process and result in the disappearance of the regular vortex street pattern.

Based on a physical discussion of the mechanics of the formation region, Gerrard (1966) has proposed that there are two simultaneous characteristic lengths, the scale of the formation region (L_f) and the width to which the free shear layers diffuse (l), which are the basis for the determination of the Strouhal frequency, namely, $St \propto (L_f l)^{-1}$. Interestingly, present results suggest that increasing of the secondary flow speed in the base region of the cylinder can disturb the separating free shear layers in such a manner that it has the same effect as increasing the disturbance level in the free stream has upon the diffusion length l. An additional possibility is that the vorticity introduced by the shear flow also disturbs the separated free shear layers

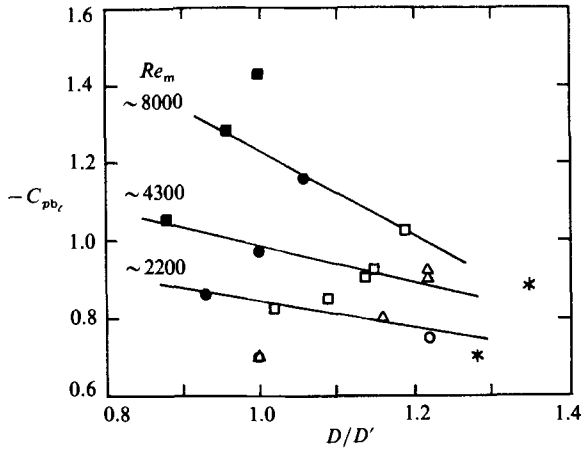

FIGURE 11. Base-pressure coefficient versus inverse of wake width.

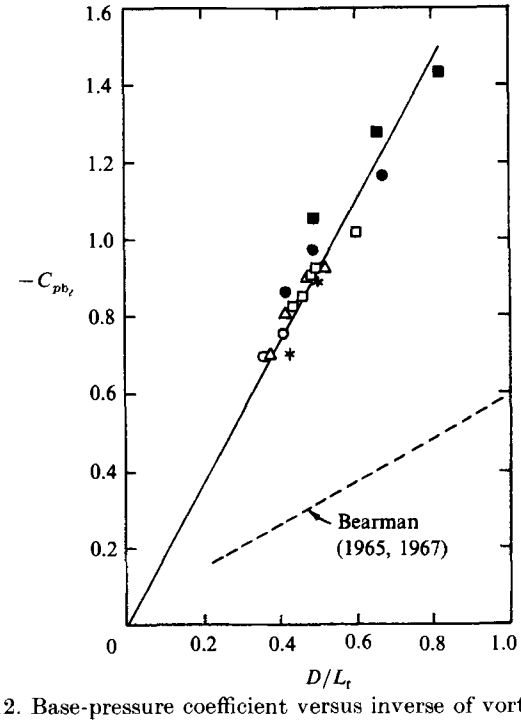

FIGURE 12. Base-pressure coefficient versus inverse of vortex-formation length.

similarly to disturbances caused by increasing the Reynolds number. For the cases of approximately constant Reynolds numbers shown in figure 10, as the steepness factor β_m increases the formation length remains the same, but owing to thickening of the free shear layers the Strouhal number decreases as indicated. For constant β_m, as Re_m increases L_f decreases and the factor l increases. These two major frequency-determining factors tend to affect the vortex-shedding frequency in opposite ways; therefore relative constancy of the Strouhal number is maintained. Figure 10 shows that St does not decrease monotonically as β_m increases. Instead St shows a tendency to approach a constant value as β_m increases.

Along the leading edge of the cylinder, the streamline will be deflected downward

owing to the existence of the pressure gradient. Fluid particles with higher velocity will be forced downward and therefore should increase the local stagnation pressure. Thus, in a shear-flow case, the local stagnation pressure coefficient should be higher than that of a uniform-flow case. The front-stagnation-pressure coefficient C_{pf_m} is defined as $(P_f - P_\infty)/(0.5\rho U_m^2)$, where P_f is the front stagnation pressure measured at a point on the nominal stagnation line. However, results of front-stagnation-pressure measurements shown in table 2 indicate that this effect is very small. The measured front-stagnation-pressure coefficients are all practically equal to 1.0, except for the large cylinders at a higher Reynolds number, when this effect becomes more pronounced. As mentioned earlier, the geometrical shape of the circular cylinder and the periodic shifting of the front stagnation line make the approaching fluid particles flow quickly around either side of the cylinder before they have moved downward very far. Nevertheless, owing to the continuous extraction of fluid from the base region of the cylinder, it is believed that the overall effect of the spanwise secondary flows will increase the local drag force and hence the local drag coefficient.

The strength of the shed vortices has long been associated with the strength of the drag force. Wood (1964) has found that a decrease in profile drag caused by base bleeding is associated with a decrease in the strength of the vortex street. Owing to greater diffusion of the free shear layer in the shear-flow case, according to Gerrard (1966) 'greater diffusion of the vorticity will result in less entrainment into the growing vortex'; hence, the strength of the shed vortices should be stronger. This is in agreement with our previous discussion that in the shear-flow situation, the drag force should be greater than that of uniform flow.

4. Conclusions

For a circular cylinder spanned vertically in a constant-shear flow with horizontal vorticity, pressure gradients generated by interaction of the shear flow with the cylinder cause a downward spanwise velocity along the leading edge of the cylinder and an upward spanwise velocity on the lee side of the cylinder. This upward mean flow velocity of the secondary flow was found to be as high as 0.44 of the mean flow velocity

The boundary layers on the wind-tunnel walls, the horseshoe vortices, and the secondary flows along the cylinder all induce end effects at junctions of the test cylinder and tunnel surfaces. Methods of using end plates, leaving gaps at junctions of the cylinder and end plates, and suction were applied to minimize the end effects.

The local base-pressure coefficient outside the regions dominated by end effects was found to be essentially constant and not affected by the local Reynolds number and local steepness factor. However, there is a systematic shift in the value of local base pressure coefficient due to the difference in Reynolds number and the steepness factor based on the midheight approach-flow speed.

For Reynolds numbers between 800 and 1.4×10^4 and a range of the steepness factor from 0.017 to 0.096, the test results indicate:

(i) With a constant steepness factor, an increase of Reynolds number has no significant effect on the Strouhal number. However, decrease of the vortex-formation length, wake width, and base-pressure coefficient results.

(ii) Increase of the steepness factor does not cause significant changes in the wake-formation length, if Reynolds number is kept invariant. In this case an increase of the wake width and a decrease of the base-pressure coefficient and the Strouhal number results.

The secondary flow on the lee side of the cylinder may be regarded as negative base bleeding which acts as a wake interference mechanism.

Part of this work was carried out under a research project funded by the Civil Engineering Laboratory, Naval Construction Battalion Center, Port Hueneme, California under contract N68305-78-C-005.

REFERENCES

BEARMAN, P. W. 1965 Investigation of the flow behind a two-dimensional model with a blunt trailing edge and fitted with splitter plates. *J. Fluid Mech.* **21**, 241.

BEARMAN, P. W. 1967 The effect of base bleed on the flow behind a two-dimensional model with a blunt trailing edge. *Aero. Q.* **18**, 207.

BEARMAN, P. W. 1970 Corrections for the effect of ambient temperature drift on hot-wire measurements in incompressible flow. *DISA Information Bull.* 11.

BLOOR, M. S. 1963 The transition to turbulence in the wake of a circular cylinder. *J. Fluid Mech.* **19**, 290.

BLOOR, M. S. & GERRARD, J. H. 1966 Measurements on turbulent vortices in a cylinder wake. *Proc. R. Soc. Lond.* **294**, 319.

GERRARD, J. H. 1965 A disturbance-sensitive Reynolds number range of the flow past a circular cylinder. *J. Fluid Mech.* **22**, 187.

GERRARD, J. H. 1966 The mechanics of the formation region of vortices behind bluff bodies. *J. Fluid Mech.* **25**, 401.

GRIFFIN, O. M. & RAMBERG, S. E. 1974 The vortex-street wakes of vibrating cylinders. *J. Fluid Mech.* **66**, 553.

GRIFFIN, O. M. & VOTAW, C. W. 1972 The vortex street in the wake of a vibrating cylinder. *J. Fluid Mech.* **51**, 31.

HAWTHORNE, W. R. 1954 The secondary flow about struts and airfoil. *J. Aero. Sci.* **21**, 588.

KÁRMÁN, T. VON & TSIEN, H. S. 1945 Lifting line theory for a wing in non-unform flow. *Q. Appl. Maths* **3**, 1.

MAIR, W. A. & STANSBY, P. K. 1975 Vortex wakes of bluff cylinders in shear flow. *SIAM J. Appl. Maths* **28**, 519.

MASKELL, E. C. 1965 A theory of the blockage effects on bluff bodies and stalled wings in a closed wind tunnel. *ARC R&M* 3400.

MAULL, D. J. & YOUNG, R. A. 1973 Vortex shedding from bluff bodies in a shear flow. *J. Fluid Mech.* **60**, 401.

ROSHKO, A. 1954 On the drag and shedding frequency of two-dimensional bluff bodies. *NACA Tech. Note* 3169.

SQUIRE, H. B & WINTER, K. G. 1951 The secondary flow in a cascade of airfoils in a non-uniform stream *J. Aero. Sci.* **18**, 271.

STANSBY, P. K. 1974 The effects of end plates on the base pressure coefficient of a circular cylinder. *Aero. J.* **78**, 36.

STARR, M. R. 1966 The characteristics of shear flows past a circular cylinder. Ph.D. thesis, University of Bristol, Bristol, UK.

TOEBES, G. H. 1969 The unsteady flow and wake near an oscillating cylinder. *Trans. ASME* D: *J. Basic Engng* **91**, 493.

TOOMRE, A. 1960 The viscous secondary flow ahead of an infinite cylinder in a uniform parallel shear flow. *J. Fluid Mech.* **7**, 141.

WOO, H. G. C., CERMAK, J. E. & PETERKA, J. A. 1989 Some studies on vortex shedding from stationary circular cylinders and oscillating cables in constant shear flow, Part 1: Stationary circular cylinders, (submitted for publication).

WOOD, C. J. 1964 The effect of base bleed on a periodic wake *J. R. Aero. Soc.* **68**, 477.